




Chiral symmetry in non-Hermitian systems: Product rule and Clifford algebraJose D. H. Rivero  and Li Ge **Department of Physics and Astronomy, College of Staten Island, CUNY, Staten Island, New York 10314, USA
and The Graduate Center, CUNY, New York, New York 10016, USA* (Received 13 May 2020; revised 25 December 2020; accepted 4 January 2021; published 19 January 2021)

Chiral symmetry provides the symmetry protection for a large class of topological edge states. It exists in non-Hermitian systems as well, and the same anticommutation relation between the Hamiltonian and a linear chiral operator, i.e., $\{H, \Pi\} = 0$, now warrants a symmetric spectrum about the origin of the complex energy plane. Utilizing two general approaches to identify and generate chiral symmetry, we first show that its symmetry operator in non-Hermitian systems can go beyond simple spatial transformations such as parity or rotation and include imaginary gauge transformations in a systematic way. Furthermore, we reveal hidden non-Hermitian chiral symmetry and its associated particle-hole symmetry, where their operators take unfamiliar forms due to the presence of energy nonconserving elements. Finally, our implementation of non-Hermitian chiral symmetry in a topological lattice leads to an edge state with “folded” localization, where its tail is reflected by the opposite edge and resides on a separate sublattice.

DOI: [10.1103/PhysRevB.103.014111](https://doi.org/10.1103/PhysRevB.103.014111)**I. INTRODUCTION**

The importance of symmetries in physics has been established in many forms, such as in Noether’s theorem that assigns a conservation law to every continuous symmetry of a system [1–3]. Outside of the quantum realm, Hermiticity is not required in general and non-Hermitian symmetries have been energetically exploited [4–6], especially since the seminal work by Bender and co-workers on parity-time (\mathcal{PT}) symmetry [7]. Several other non-Hermitian symmetries have also been carefully analyzed, such as the non-Hermitian extensions of particle-hole and chiral symmetries [8–12], as well as exclusively non-Hermitian symmetries including pseudo-Hermiticity [13] and pseudochirality [3].

Among them, chiral symmetry is one of particular interest in topological systems, for it provides protection to a wide range of topological states in Hermitian systems [14–20]. Originally conceived to describe the conserved handedness of Dirac fermionic fields, it often accounts for the symmetry of the energy bands with respect to the Fermi level or the energy of an uncoupled orbital. A natural non-Hermitian extension of chiral symmetry can be introduced via the same anticommutation relation between the Hamiltonian and a linear operator, which now warrants a complex spectrum symmetric about the origin of the complex energy plane [8]. As a consequence, a non-Hermitian zero mode, with its energy right at the origin of the complex plane, can still exist similar to its Hermitian counterpart. Such exotic states and associated topological phases of matter have attracted fast-growing interest in photonics and related fields [21–35], which are inherently open systems and demand a systematic study and characterization of non-Hermitian chiral symmetry.

Several important differences exist among the consequences of chiral symmetry in Hermitian and non-Hermitian systems. In the latter, the pairwise eigenstates of the system warranted by chiral symmetry not only have opposite frequencies (given by the real part of the energy eigenvalues), but they also have opposite gain and loss (given by the imaginary part of the energy eigenvalues). In addition, unlike the chiral symmetry in a Hermitian lattice with two sublattices, the zero modes in a non-Hermitian lattice are not found to have finite amplitudes in only one sublattice in general. Furthermore, these zero modes can be exceptional points (EPs) [36–43] where two or more eigenstates coalesce with the same wave function, a unique property in non-Hermitian systems.

On the one hand, the easiest way to construct a non-Hermitian system with chiral symmetry is to maintain the sublattice symmetry of an underlying Hermitian system (such as in a tight-binding square or honeycomb lattice without on-site detunings) and lift its Hermiticity by introducing asymmetric couplings [9]. While this approach can be applied to both periodic [8] and finite-size systems, it does not utilize one important benefit provided by the non-Hermitian platforms in optics and photonics [4], namely, the availability and tunability of gain and loss in optical cavities and waveguides, which are represented by an imaginary detuning between different lattice sites. On the other hand, if we directly apply such an imaginary detuning to a Hermitian system with chiral symmetry, its chiral symmetry is lifted and we often obtain non-Hermitian particle-hole (NHPH) symmetry [9–11] or pseudo-anti-Hermiticity [3,44] instead, which results in a spectrum symmetric about the imaginary axis of the complex energy plane [8,45].

To overcome these obstacles and facilitate the exploration of topological phases of matter in non-Hermitian systems, two general approaches can be employed to identify and generate non-Hermitian chiral symmetry. In the first approach, a product rule where chiral symmetry, denoted by Π below, results

*li.ge@csi.cuny.edu

from the simultaneous satisfaction of NHPH symmetry and bosonic antilinear symmetry. The former is defined similarly to its Hermitian counterpart, i.e., with the Hamiltonian H anti-commuting with an antilinear operator Ξ ; the latter is defined as a commutation relation between the Hamiltonian and an antilinear operator Λ , with \mathcal{PT} symmetry being a prominent example. In the second approach, the Clifford algebra satisfied by the Dirac matrices can be utilized to discover and analyze non-Hermitian chiral symmetry, independent of NHPH and bosonic antilinear symmetries.

In this paper, we employ these two approaches to broaden our knowledge of non-Hermitian chiral symmetry. We first show that its operator does not necessarily only involve simple spatial transformations, such as parity or rotation in a two-dimensional (2D) lattice. In particular, we show how imaginary gauge transformations [46–48] can be included in a systematic way while maintaining non-Hermitian chiral symmetry, exemplifying flexible control of non-Hermitian zero modes at an EP and achieving spatial localization at the center, one corner, or all corners of a square lattice. Furthermore, we reveal hidden non-Hermitian chiral symmetry and its associated NHPH symmetry, where their operators take unfamiliar forms due to the presence of energy nonconserving elements. Finally, our implementation of non-Hermitian chiral symmetry in a topological lattice with complex detunings leads to an edge state with “folded” localization, where its tail is reflected by the opposite edge and resides on a separate sublattice.

II. APPROACH I: PRODUCT RULE

We first review two important concepts in the fundamental proposition regarding possible forms of symmetries in quantum systems, i.e., the Wigner theorem [49]. It states that any symmetry transformation is necessarily represented by a linear (and unitary) or antilinear (and antiunitary) transformation of the Hilbert space. A linear symmetry transformation \mathcal{U} satisfies

$$\mathcal{U}(a\phi_1 + b\phi_2) = a\mathcal{U}\phi_1 + b\mathcal{U}\phi_2, \quad (1)$$

where $\phi_{1,2}$ are two arbitrary quantum states and the complex numbers a, b are their linear superposition coefficients. In contrast, an antilinear symmetry operator \mathcal{A} satisfies

$$\mathcal{A}(a\phi_1 + b\phi_2) = a^*\mathcal{A}\phi_1 + b^*\mathcal{A}\phi_2, \quad (2)$$

where the asterisks denote the complex conjugation as usual. From this definition, it can be inferred that an antilinear operator can be represented by the product of a linear operator and the complex conjugation.

As mentioned in the Introduction, the first approach we employ to generate non-Hermitian chiral symmetry relies on the simultaneous satisfaction of NHPH symmetry and a non-Hermitian bosonic antilinear symmetry:

$$\{H, \Xi\} = 0, \quad [H, \Lambda] = 0. \quad (3)$$

Bosonic antilinear symmetry can be implemented conveniently using strategically placed photonic elements with balanced optical gain and loss [4]. Meanwhile, a probably more important and intriguing foundation of this approach is that imposing any arbitrary imaginary on-site potentials to an underlying Hermitian chiral lattice with real-valued couplings

gives rise to NHPH symmetry automatically [9]. Therefore, NHPH symmetry can coexist nicely with bosonic antilinear symmetry enabled by optical gain and loss, which in turn warrants non-Hermitian chiral symmetry as we show in detail below.

Since both Ξ and Λ in Eq. (3) are antilinear operators, they can be written as the product of a linear operator and the complex conjugation K :

$$\Xi \equiv CK, \quad \Lambda \equiv XK. \quad (4)$$

K is often the manifestation of time-reversal operator for a finite-sized system [7], and C for the NHPH symmetry mentioned above is given by the chiral operator of the underlying Hermitian lattice, i.e., $C = P_A - P_B$ as in the Su-Schrieffer-Heeger (SSH) model [50], where $P_{A,B}$ are the projection operators onto the two sublattices. These two sublattices are defined such that there is no coupling between two sites on the same sublattice. X , on the other hand, can take a variety of forms. For example, two common choices of X in 2D are mirror reflection and rotation, which lead to \mathcal{PT} [4–7] and rotation-time (\mathcal{RT}) symmetry [51–53], respectively.

As a consequence of Eq. (3), the following symmetry transformations hold for the eigenstates of H ,

$$\Xi\psi_\mu = \psi_\nu, \quad \Lambda\psi_\nu = \psi_{\nu'}, \quad (5)$$

where the subscripts μ, ν, ν' are not necessarily the same. The corresponding energy eigenvalues satisfy

$$\varepsilon_\mu = -\varepsilon_\nu^*, \quad \varepsilon_\nu = \varepsilon_{\nu'}^*, \quad (6)$$

i.e., they are symmetric about the imaginary and real energy axis of the complex energy plane, respectively. It is then straightforward to see

$$\Lambda\Xi\psi_\mu = \psi_{\nu'}, \quad \varepsilon_\mu = -\varepsilon_{\nu'}, \quad (7)$$

which indicates the existence of chiral symmetry, i.e., $\{H, \Pi\} = 0$, with the *linear* operator $\Pi \equiv \Lambda\Xi = XC^*$. A non-Hermitian zero mode occurs when all the subscripts are the same, leading to $\varepsilon_\mu = 0$.

This product rule is similar in construction to how chiral symmetry in a Hermitian system can be generated as the product of particle-hole symmetry and time-reversal symmetry [14]. However, we note that since the non-Hermitian chiral operator Π is no longer given by the difference of the sublattice projection operators, the wave function of a non-Hermitian zero mode with $\varepsilon_\mu = 0$ does not necessarily vanish on one sublattice. More importantly, this zero energy can be an EP as mentioned in the Introduction. Further discussion on these properties can be found in Appendix A.

The product rule discussed above exists in previously studied systems where the bosonic antilinear symmetry involves a simple spatial transformation, such as parity or rotation that is represented by a permutation in the matrix form [8]. However, this product rule is much more general, and in some cases the bosonic antilinear symmetry, as well as the NHPH symmetry, is complicated and often hidden.

As an example, let us contrast two one-dimensional lattices shown in Figs. 1(a) and 1(d). They have the same pair of gain and loss of the same strength (i.e., with imaginary on-site potentials $\pm i\tau$) at the two ends, but system I has symmetric coupling while system II has asymmetric couplings. These

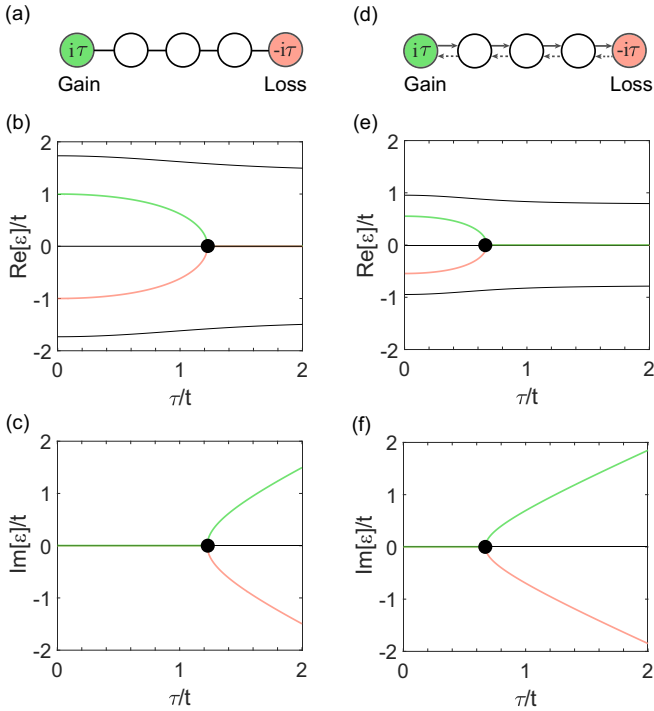


FIG. 1. Generating non-Hermitian chiral symmetry by the product rule. (a), (d) Schematics of two tight-binding lattices. Solid and dashed links indicate couplings $t \in \mathbb{R}$ and $t' = 0.3t$. (b), (c) Real and imaginary parts of the complex spectrum for the lattice in (a) as a function of the gain and loss strength τ . The black dot marks its exceptional point. (e), (f) Same as (b), (c) but for the lattice in (d).

lattices can be realized using optical microcavities and their counterparts in microwaves, acoustics, and other related fields [4]. In particular, asymmetric couplings of different magnitudes can be achieved by introducing auxiliary rings [54]. In this scheme, each lattice is represented an optical microring cavity, and two such cavities are coupled via a third ring that has optical gain and loss in its two halves, respectively. When the clockwise (CW) circulating light in the left microring travels to the third ring in the middle, it goes through the *bottom* half of the ring before coupling to the CW circulating light in the right cavity. When this process is reversed, the CW light in the right microring travels to the *top* half of the middle ring instead, before coupling to the CW light in the left microring. Therefore, by having gain and loss in the top and bottom halves of the middle ring, respectively, light is amplified along one semicircle and attenuated along the other, hence making the couplings of the left and right cavities asymmetric. This scheme of asymmetric couplings has been realized using two microring resonators with InGaAsP multiple quantum wells [48], which is captured well by a tight-binding model. Extending this approach to a lattice with more sites does not require additional fabrication techniques and hence should be undemanding.

When τ is zero in Fig. 1, both systems have sublattice symmetry and hence chiral symmetry as well. When τ becomes nonzero, system I acquires NHPH symmetry as specified in Eq. (4) and \mathcal{PT} symmetry with the parity operator \mathcal{P} performing a horizontal mirror reflection. Therefore, it displays

a symmetric spectrum about the origin in the complex energy plane [Figs. 1(b) and 1(c)], manifesting its non-Hermitian chiral symmetry explained by the product rule given by Eq. (7). While the same route to NHPH symmetry still applies in system II with $\Xi = CK$, system II clearly lacks \mathcal{PT} symmetry due to the asymmetric couplings. Therefore, it is quite remarkable that the system still displays a symmetric spectrum in the complex energy plane [Figs. 1(e) and 1(f)].

To understand this behavior, we note that asymmetric couplings can be regarded as a consequence of an imaginary gauge transformation [46]. However, previous investigations of such gauge transformations have excluded explicitly gain and loss, which by far is the most viable approach to realize non-Hermitian systems in photonics and related areas [4]. Here, in the presence of the gain and loss cavity in system II, the imaginary gauge transformation, given by

$$\psi_n = e^{-\frac{1-n}{2} \ln \frac{t}{t'}} \tilde{\psi}_n \equiv s^{n-1} \tilde{\psi}_n, \quad (8)$$

from a system with symmetric coupling $\tilde{t} = \sqrt{tt'}$ and wave function $\tilde{\psi}_n$ in the n th cavity, *preserves* the strength of gain and loss. As a result, the operator X in the bosonic antilinear symmetry is given by

$$X = GPG^{-1}, \quad G = \text{diag}(1, s, s^2, \dots), \quad (9)$$

where \mathcal{P} is the same mirror reflection as in system I. Clearly, X is a linear operator and $X^2 = G\mathcal{P}^2G^{-1} = \mathbf{1}$, where $\mathbf{1}$ is the identity matrix. Together with the aforementioned NHPH symmetry, the non-Hermitian chiral symmetry of system II is then given by $\Pi = XC = GPG^{-1}C = GPCG^{-1}$, where we have used $[G^{-1}, C] = 0$ for these two diagonal operators.

The imaginary gauge transformation given by Eq. (8) is characterized a phase $\phi = i\frac{1-n}{2} \ln \frac{t}{t'}$ that is linear in space. This property leads to asymmetric couplings that are homogeneous in space, i.e., t and t' in system II. More generally, the gauge transformation can involve a phase with a more complicated spatial dependence. In particular, one can localize a zero mode that is at an EP and protected by non-Hermitian chiral symmetry anywhere in the system with ease.

Figure 2(a) shows one example in a square lattice with nine rows and columns, and gain and loss are imposed in the leftmost and rightmost columns. To apply the imaginary gauge transformation, we let the asymmetric horizontal and vertical couplings be t, t' and $1.1t, 1.1t'$, respectively. In Fig. 2(b), these asymmetric couplings are still homogeneous in space, and an EP of order 3 [55–58] is reached at $\tau = 0.79t$, similar to those in Fig. 1. The corresponding wave function is exponentially localized at the upper right-hand corner. If instead we exchange the two asymmetric couplings in the x (y) direction in the right (bottom) half of the lattice, the EP is realized at $\tau = 0.94t$, and the non-Hermitian zero mode is localized at the defect of the gauge transformation in both directions, i.e., right at the middle of the square lattice [Fig. 2(c)]. Finally, if we reverse the direction of all these asymmetric couplings, now the non-Hermitian zero mode at its EP is localized at all four corners [Fig. 2(d)], reached when $\tau = 0.7t$.

Here, we note that even though the system remains non-Hermitian when the gain and loss are removed, it can be obtained from a Hermitian system with uniform couplings

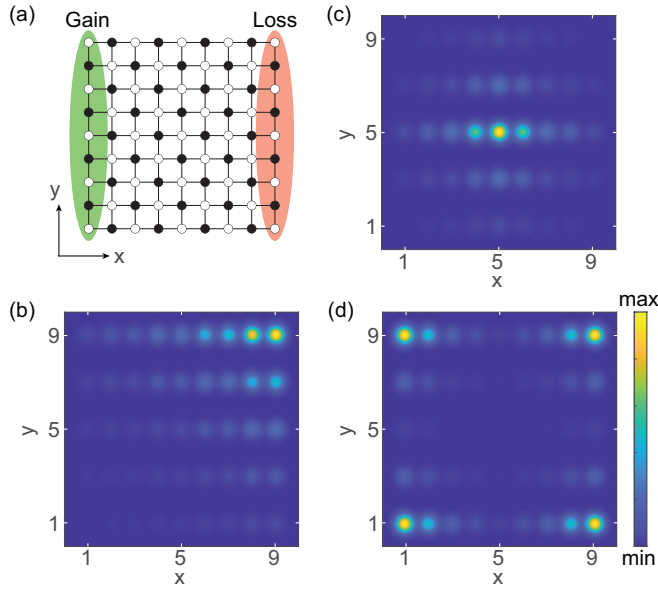


FIG. 2. Localized non-Hermitian zero mode at an EP. (a) Schematic of a square lattice before an imaginary gauge transformation is applied. Horizontal and vertical couplings are given by t and $1.1t$, respectively. (b)–(d) Spatial profile of a zero mode at an EP with a modified coupling $t' = 0.7t$, $0.5t$, and $0.4t$, respectively. See the main text for the application of this imaginary gauge transformation.

$\sqrt{tt'}$, $\sqrt{1.1tt'}$ in the x and y direction, respectively, similar to the imaginary gauge transformation mentioned below Eq. (8). Therefore, such a system without gain and loss always has a real-valued energy spectrum and cannot have an EP, unless a periodic boundary condition is imposed [46], which is difficult to imagine in 2D and breaks down the imaginary gauge transformation. With the introduction of gain and loss with the imaginary gauge transformation, however, the chiral symmetry-induced zero mode at an EP demonstrated here may lead to applications in enhanced optical and photonic sensing [58–60].

In these examples, the imaginary gauge transformation does not affect NHPH symmetry: The transformed lattices by the imaginary gauge still consist of two sublattices with real couplings, and the imaginary on-site detunings due to gain and loss again lead to NHPH symmetry [9]. Therefore, one just needs to analyze the spatial dependence of the phase ϕ to identify Ξ accountable for its bosonic antilinear symmetry. This task becomes increasingly more difficult with the system size if the variation of ϕ is complex or even random.

In the meanwhile, there are other systems with non-Hermitian chiral symmetry where it is NHPH symmetry that is obscure. For example, one may accidentally construct systems with NHPH and non-Hermitian chiral symmetries [61] and be unaware of their symmetry operators. One such case is given in Fig. 3(a), where four sites on a tight-binding ring are coupled by two pairs of complex couplings, g_1 and g_2 ; this model can be considered as a generalized Rice-Mele model [62], with the two sites on the diagonal detuned from the other two on the antidiagonal by 2Δ . When Δ is real, it can be shown that the eigenvalues of this system are symmetric about

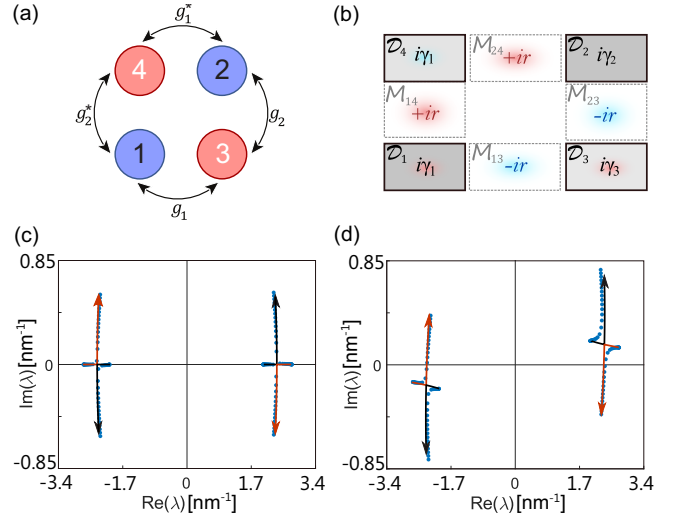


FIG. 3. A hidden non-Hermitian chiral symmetry. (a) Schematic of a four-cavity ring with complex couplings $g_1 \equiv g_{1r} + ig_{1i}$, $g_2 \equiv g_{2r} + ig_{2i}$, and their complex conjugates. Blue and orange denote the on-site detunings $\pm\Delta$. (b) Cross section of four coupled waveguides embedded in a silica substrate that emulate the tight-binding model shown schematically in (a). The four waveguides are denoted by \mathcal{D}_{1-4} , and the rectangular regions between two nearest neighbors are denoted by \mathcal{M}_{13} , \mathcal{M}_{14} , \mathcal{M}_{23} , \mathcal{M}_{24} . Complex couplings g_1 and g_2 are achieved by locally introducing gain ($-ir$ in the dielectric constant) in \mathcal{M}_{13} , \mathcal{M}_{23} , while g_1^* and g_2^* are implemented by loss (ir in the dielectric constant) in \mathcal{M}_{14} , \mathcal{M}_{24} . (c), (d) Trajectories of the complex eigenvalues λ in the paraxial equation when r is increased from 0 to 0.009 with (c) $\Delta = 1.1216 \text{ nm}^{-1}$ and (d) $\Delta = 1.1216 + 0.6990i \text{ nm}^{-1}$. Black dots show finite-difference simulations of (b), which are captured qualitatively by the tight-binding model (thick solid lines). The arrows indicate the motion of λ 's with increasing r , and the real and imaginary axes are shown as thin solid lines. The parameters of the tight-binding model used are $g_{1i} = -2.3895r \text{ nm}^{-1}$, $g_{2i} = -18.648r \text{ nm}^{-1}$, $g_{1r} = 0.4107 \text{ nm}^{-1}$, $g_{2r} = 2.1054 \text{ nm}^{-1}$. They give the best fit for the trajectories of the finite-difference solutions of the paraxial equation.

the real axis, imaginary axis, and the origin of the complex plane. The first property is the result of \mathcal{RT} symmetry: The system is invariant under a combined π -rotation and time-reversal operation when β is real. The NHPH symmetry, on the other hand, is difficult to identify and cannot be revealed using a gauge transformation. To pin down this accidentally generated NHPH symmetry and the resulting non-Hermitian chiral symmetry, we change the perspective in Sec. III and resort to the second approach mentioned in the Introduction, i.e., the Clifford algebra and the Dirac matrices.

Here, we note a scheme to realize non-Hermitian couplings $g_{1,2}$ in the model above by embedding photonic elements (e.g., resonators or waveguides) in amplifying or absorbing media [63]. We implement this scheme in Fig. 3(b) using the transverse-electric (TE) modes in four coupled silica waveguides, which emulate the tight-binding model in Fig. 3(a) via a coupled-mode analysis (see the details in Appendix B). These waveguides are formed by a small contrast in the real part of the refractive index from the background silica, i.e., 1.4586 in waveguides 1 and 2 and 1.4594 in waveguides 3 and 4 vs

1.449 in the substrate at the telecom wavelength $1.550 \mu\text{m}$. Even though the index contrast is low, a guided mode inside the waveguides only requires an incident angle larger than the critical angle of 83° in this case, which is satisfied here in the paraxial regime: The propagation constants of these modes are found to be about $5.88 \mu\text{m}^{-1}$, leading to an incident angle of 84° that is just above the critical angle. We denote the eigenvalues of the paraxial equation in this case by λ 's, which are in the unit of μm^{-1} . They correspond to the eigenvalues ε of the tight-binding Hamiltonian shown schematically in Fig. 3(a) [see also Eq. (16)]. By solving for λ 's in the coupled system using finite-difference simulations, we find qualitative agreement between these results and the ones produced by the coupled-mode analysis, as can be seen by comparing the dots and solid lines in Figs. 3(c) and 3(d), respectively. The (approximate) non-Hermitian chiral symmetry of this system is readily seen in both figures, where the detuning Δ is real and imaginary, respectively. The absence of other symmetries in the latter case will be discussed in the next section, and details of the simulations can be found in Appendix B.

III. APPROACH 2: CLIFFORD ALGEBRA

The Dirac matrices $\{\gamma^0, \gamma^1, \gamma^2, \gamma^3\}$, also known as the gamma matrices, appear in the Dirac equation to describe relativistic quantum mechanics. They are given by

$$\gamma^0 = \begin{pmatrix} \mathbf{1}_2 & 0 \\ 0 & -\mathbf{1}_2 \end{pmatrix}, \quad \gamma^j = \begin{pmatrix} 0 & \sigma_j \\ -\sigma_j & 0 \end{pmatrix} \quad (j = 1, 2, 3), \quad (10)$$

in terms of the identity matrix and Pauli matrices. Together with

$$\gamma^5 = \begin{pmatrix} 0 & \mathbf{1}_2 \\ \mathbf{1}_2 & 0 \end{pmatrix}, \quad (11)$$

they satisfy the Clifford algebra

$$\{\gamma^\mu, \gamma^\nu\} = 0 \quad (\mu \neq \nu), \quad \{\gamma^\mu, \gamma^\mu\} = 2\xi^\mu \mathbf{1}_4, \quad (12)$$

where $\xi^\mu = 1$ ($\mu = 0, 5$) and -1 ($\mu = 1, 2, 3$). This defining property of the Clifford algebra is particularly appealing in the generation of non-Hermitian chiral symmetry: By defining the Hamiltonian as a superposition of the Dirac matrices and their products, we have a straightforward way to determine its chiral operators.

For example, if the Hamiltonian includes a linear superposition (with arbitrary coefficients g_i and g_j) of individual Dirac matrices, we can enumerate all its chiral symmetries by using Eq. (12) as well as

$$\{g_i \gamma^i + g_j \gamma^j, \xi^i g_j \gamma^j - \xi^j g_i \gamma^i\} = 0 \quad (i \neq j) \quad (13)$$

and

$$\{\gamma^j \gamma^k, \gamma^l\} = 0, \quad (14)$$

where $j \neq k$ and $l = j$ or k . If the Hamiltonian also contains the product of two Dirac matrices, we may also need to utilize

$$\{\gamma^j \gamma^k, \gamma^l \gamma^m\} = 0 \quad (j \neq l \neq k). \quad (15)$$

In this analysis, we note that on-site detunings can be expressed by $\gamma^0 = \text{diag}(1, 1, -1, -1)$, $i\gamma^1 \gamma^2 = \text{diag}(1, -1, 1, -1)$, $\gamma^3 \gamma^5 = \text{diag}(1, -1, -1, 1)$, and

the trivial uniform detuning $\mathbf{1}_4$, as well as their linear superpositions.

Now let us revisit the system shown in Fig. 3(a). Its Hamiltonian can be written as

$$H = \Delta \gamma^0 + g_{1r} \gamma^5 + \gamma^0 (g_{2r} \gamma^1 + i g_{1i} \gamma^3) + g_{2i} \gamma^2, \quad (16)$$

where $g_1 \equiv g_{1r} + i g_{1i}$ and $g_2 \equiv g_{2r} + i g_{2i}$. In the absence of detuning (i.e., $\Delta = 0$), we find γ^0 as a chiral operator, which is identical to the sublattice operator C in Eq. (4). Note, however, it is not the only chiral operator in this case. Using a generalization of Eq. (14), i.e.,

$$\{\gamma^j \tilde{\gamma}, \tilde{\gamma}\} = 0, \quad \tilde{\gamma} = \sum_{k \neq j} a_k \gamma^k, \quad (17)$$

we find another chiral operator given by

$$\Pi = g_{2r} \gamma^1 + i g_{1i} \gamma^3 \quad (18)$$

with proper normalization.

The non-Hermitian chiral symmetry defined by this Π operator holds even when Δ is *finite*, whereas that defined by γ^0 (i.e., the sublattice symmetry) is lifted. Π then warrants the spectrum symmetry about the origin of the complex energy plane observed in Fig. 3(c). In the case that Δ is real, the system also has \mathcal{RT} symmetry as mentioned. From the perspective of the product rule discussed previously, i.e., $\Pi = \Lambda \Xi$, one can then identify the obscure NHPH symmetry as

$$\Xi = \mathcal{R}_2 K (g_{2r} \gamma^1 + i g_{1i} \gamma^3) = \mathcal{R}_2 (g_{2r} \gamma^1 - i g_{1i} \gamma^3) K. \quad (19)$$

This NHPH symmetry, as well as the \mathcal{RT} symmetry, is lifted with a complex Δ . However, the non-Hermitian chiral symmetry persists owing to the Clifford algebra [Fig. 3(d)].

In the example above, the sublattice symmetry is lifted by a finite detuning. It also disappears with next-nearest-neighbor (NNN) couplings [i.e., between cavities of the same color arranged diagonally in Fig. 3(a)], but in this case non-Hermitian chiral symmetry can still be introduced by using the Clifford algebra in principle (see Appendix C).

A remarkable advantage of the Clifford algebra approach emerges when intricate forms of detunings and coupling constants are to be implemented in photonic lattices. Therefore, it facilitates the investigation of non-Hermitian extensions of known Hermitian topological systems. Below, we exemplify this approach and show a phenomenon of “folded” localization.

An interesting family of topological tight-binding Hermitian lattices were constructed as nontrivial square roots of some parent systems in Ref. [64]. Despite the lack of sublattice symmetry in the parent systems, the resulting lattices feature bands symmetric about the zero energy and acquire their topological properties from band inversions protected by chiral symmetry. In particular, the Bloch Hamiltonian of the Hermitian “bow-tie” lattice [64] can be written as

$$H_s = (\beta \gamma^0 + i g_2 \gamma^1 \sin k - i g_2 \gamma^2 \cos k) + g_3 \gamma^1 \gamma^5, \quad (20)$$

where $\beta, g_{1,2}$ are all real couplings and k is the lattice wave vector. This model has been realized using coupled silicon waveguides [65].

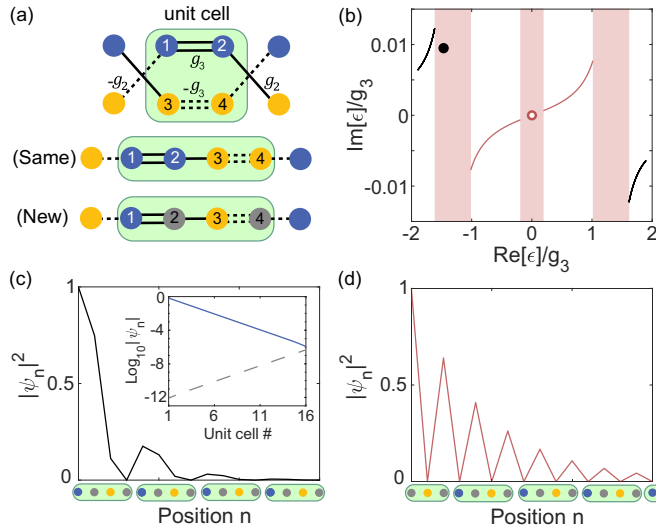


FIG. 4. Non-Hermitian extension of a topological lattice. (a) Schematic of H_s given by Eq. (20) (top) and its equivalent form (middle). The bottom shows a similar lattice but with different detunings, and its complex band structure (solid lines) is shown in (b). Shaded areas represent the projection of the bulk band gaps on the real energy axis. Solid and open dots in (b) indicate the energy of the edge states in (c) and (d), respectively. They are finite in length with 64 and 63 sites, where purple, orange, and gray denote the on-site detunings $\pm\beta$ and 0. Inset in (c): Amplitude of this edge state in the first (solid) and last (dashed) cavities of all 16 unit cells. $g_2/g_3 = 0.8$ and $\beta/g_3 = -0.3 + 0.01i$ are used.

H_s in Eq. (20) actually describes two copies of the same lattice [see Fig. 4(a)], but it is easier to analyze than the Bloch Hamiltonian of the latter using the Clifford algebra. The previously identified chiral symmetry of H_s is given by γ^5 , which can be readily verified using Eqs. (12) and (14). Using Eqs. (15) and (17), we also identify another non-Hermitian chiral symmetry,

$$\Pi_2 = \frac{\gamma^1(\beta\gamma^0 - ig_2\gamma^2 \cos k)}{N^{\frac{1}{2}}}, \quad N = \beta^2 + g_2^2 \cos^2 k, \quad (21)$$

which is not found in Refs. [64,65]. Here, the product of the two chiral operators leads to a linear symmetry, i.e.,

$$\Pi_2\Pi_1 = -\frac{i\beta\gamma^2 + g_2\gamma^0 \cos k}{N^{\frac{1}{2}}} \equiv W, \quad [H, W] = 0, \quad (22)$$

and $\{1, \Pi_1, \Pi_2, W\}$ form the Klein group, which is the direct product of two Z_2 groups.

Besides γ^0 , the simple form of Π_1 also accommodates detunings of the form $\gamma^3\gamma^5$, which is given by $\text{diag}(1, -1, -1, 1)$ as mentioned previously. By itself, this form of detunings is equivalent to γ^0 , which is most obvious once we perform a gauge transformation on the wave function in the fourth cavity, i.e., $\psi_4 \rightarrow -\psi_4$; it flips the sign of all negative couplings [66], with which the difference between γ^0 and $\gamma^3\gamma^5$ lies only in the order of g_2 and g_3 . This lattice reduces to the SSH model without this form of detunings.

More importantly, the Clifford algebra analysis leads to the following two observations. First, the chiral symmetry given by Π_1 persists when these detunings are complex, which

offers a straightforward route to study the non-Hermitian extension of this model. Second, these different forms of detunings can coexist without destroying this chiral symmetry. For example, even though the detunings given by γ^0 and $\gamma^3\gamma^5$ are equivalent as mentioned, their superposition gives a different form of detuning [e.g., $\beta(\gamma^0 + \gamma^3\gamma^5) = \text{diag}(2\beta, 0, -2\beta, 0)$ as depicted in the bottom panel of Fig. 4(a)] and leads to another lattice. By taking β to be complex, we observe a complex spectrum with non-Hermitian chiral symmetry [solid lines in Fig. 4(b)]. Due to the ambiguity of defining topological numbers in non-Hermitian systems, here we avoid this discussion and show instead the evidence of topological protection, i.e., edge states in the band gaps of the system.

Depending on the terminations at the two ends of this lattice, it can display, for example, an edge state in the left band gap [solid dot in Fig. 4(b)] or right at the origin [open dot in Fig. 4(b)], i.e., a non-Hermitian zero mode. Their spatial profiles are shown in Figs. 4(c) and 4(d), respectively. While both of them seem to have vanished amplitude in a subset of cavities, only the zero mode is truly dark on one of the original sublattices before the detunings are introduced, consisting of the first and third cavities of each unit cell. The alternate detunings on this sublattice do not affect the spatial profile of this mode, and hence its energy remains zero. In contrast, the edge state shown in Fig. 4(c) has a “folded” localization: The amplitude of the wave function in the first three cavities of each unit cell attenuates exponentially from left to right, while that in the fourth cavity increases exponentially, as if the tail of this edge mode localized on the left is reflected by the opposite boundary (see the inset).

IV. CONCLUSION AND DISCUSSION

In summary, we have presented two general approaches to construct systems with non-Hermitian chiral symmetry, aiming to facilitate the exploration of topological phases of matter in non-Hermitian systems, especially on optical and photonic platforms. The first approach relies on the simultaneous satisfaction of NHPH symmetry and non-Hermitian bosonic antilinear symmetry. We have shown that by going beyond simple spatial transformations such as parity or rotation, a much broader range of non-Hermitian systems can display chiral symmetry, including those with an imaginary gauge transformation. The second approach utilizes the Clifford algebra, and the examples we have discussed are based on the Dirac matrices. They have helped us reveal non-Hermitian chiral and other symmetries whose operators would otherwise remain obscure. Using this approach, we have also investigated the non-Hermitian extension of a known topological model, and we have shown that chiral symmetry as well as topological edge states can persist with complex on-site potentials. Generalizations to more complicated or even higher-dimensional systems can also be achieved, by working with suitable Clifford algebras.

As a final clarification, we note that chiral symmetry in optics and photonics can also refer to the symmetry between clockwise and counterclockwise modes of motion [67–70], which should be distinguished from our discussions here.

ACKNOWLEDGMENT

This project is supported by the NSF under Grant No. PHY-1847240.

APPENDIX A: HERMITIAN VERSUS NON-HERMITIAN CHIRAL SYMMETRY

In the Introduction of the main text, we have listed several different consequences of chiral symmetry in Hermitian and non-Hermitian systems. Here, we exemplify these differences by considering a tight-binding honeycomb lattice with three rings and the same nearest-neighbor coupling $g \in \mathbb{R}$ everywhere [Fig. 5(a)]. Before we introduce on-site gain and loss, the system is Hermitian and its chiral symmetry warrants a symmetric spectrum about $\varepsilon = 0$ [Fig. 5(c)], with a single (and nondegenerate) zero mode that only has a finite amplitude in the sublattice B indicated by sites with solid dots [Fig. 5(e)].

For its non-Hermitian counterpart, we impose equal gain and loss (i.e., $\pm i\tau$ for the imaginary parts of the on-site

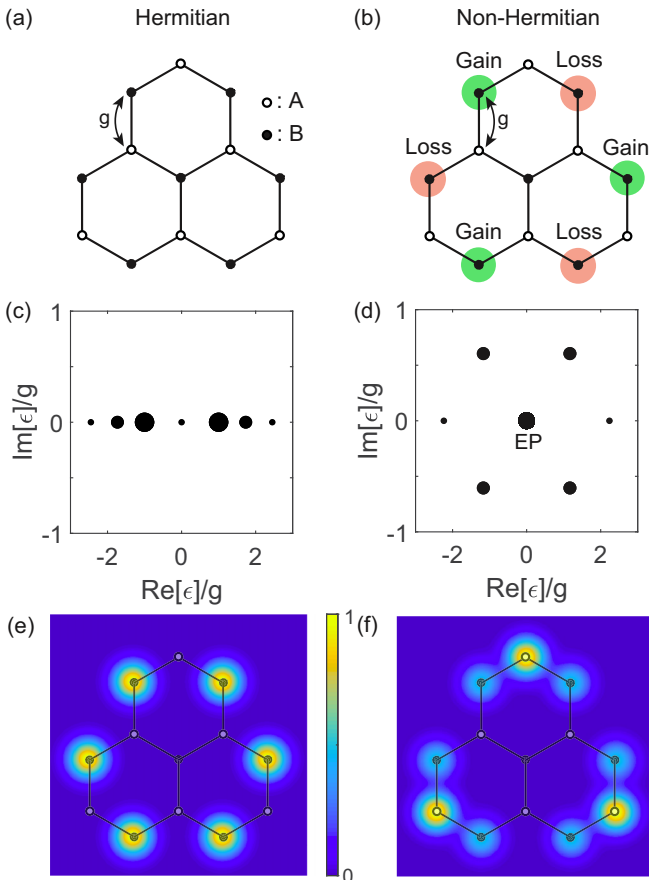


FIG. 5. Hermitian vs non-Hermitian chiral symmetry. (a) Schematic of a finite-size honeycomb lattice with only nearest-neighbor couplings. The two sublattices A and B are marked by solid and open dots. (b) Its non-Hermitian counterpart with also NHPH and \mathcal{PT} symmetries. (c), (d) Complex spectra for (a) and (b) at $\tau = \sqrt{2}g$. Dots of increasing sizes indicate nondegenerate, doubly degenerate, and triply degenerate states. (e), (f) Spatial profiles of the zero modes in (c) and (d).

potentials) to three pairs of lattice sites [Fig. 5(b)]. This system can be described by the generalized dihedral group \mathcal{MT}_{2v} ($v = 3$) [51], with all v reflections in the dihedral group D_{2v} now combined with time reversal. Therefore, we have three different parity-time operators $\Lambda_j = \mathcal{P}_j K$ ($j = 1, 2, 3$), which are about the 90° (270°), 30° (210°), and 150° (330°) axes, respectively. Since the underlying Hermitian honeycomb lattice with real-valued couplings has chiral symmetry, NHPH symmetry arises automatically with the introduced gain and loss modulation as mentioned in Sec. II, with $\Xi \equiv (P_A - P_B)K$. Together, they lead to three related non-Hermitian chiral operators specified by the product rule in Eq. (7), i.e.,

$$\Pi_j = \mathcal{P}_j(P_A - P_B), \quad (\text{A1})$$

with $\Pi_2 = \mathcal{R}_3 \Pi_1$, $\Pi_3 = \mathcal{R}_3 \Pi_2$, and $\Pi_1 = \mathcal{R}_3 \Pi_3$. Here, \mathcal{R}_n is the counterclockwise rotation by an angle equal to $360^\circ/n$.

Due to the presence of both NHPH and \mathcal{PT} symmetries, the spectrum shown in Fig. 5(d) is symmetric about the real and imaginary axes as well, which is a property when the non-Hermitian chiral symmetry is constructed using the product rule. In the absence of these other symmetries, the spectrum due to non-Hermitian chiral symmetry is only symmetric about the origin of the complex energy plane [see, for example, the solid lines in Fig. 4(b)].

When the gain and loss strength is set to $\tau = \sqrt{2}g$, this non-Hermitian system has an EP zero mode [Fig. 5(d)] where three eigenstates of H coalesce with the same wave function. Clearly, this wave function has a finite amplitude on both the A and B sublattices [Fig. 5(f)]. This property holds for any other finite value of τ , where the system has a single, non-EP zero mode.

APPENDIX B: FOUR-COUPLED WAVEGUIDE RING WITH HIDDEN CHIRAL SYMMETRY

In Sec. II of the main text, we have introduced a system with a hidden non-Hermitian chiral symmetry, consisting of a ring of four sites with real detunings and complex coupling constants. This system is emulated using a silicon-based photonic setup in Fig. 3, where we use the notion of *active coupling* between waveguides [63]: One introduces gain and loss in the surrounding medium to achieve complex coupling constants and emulate the tight-binding model in Eq. (16). In this Appendix, we obtain the parameters for the tight-binding model from a coupled-mode analysis.

The silicon waveguides [denoted by \mathcal{D}_{1-4} in Fig. 3(b) and below] have the same rectangular cross section of $5 \mu\text{m} \times 3 \mu\text{m}$ in our simulations, with two distinct refractive indices $n_1 = 1.4586$ and $n_2 = 1.4594$ arranged diagonally. They are embedded in a silica substrate with refractive index $n_{cl} = 1.449$. To produce two types of coupling constants g_1, g_1^* and g_2, g_2^* , we arrange the waveguides with horizontal and vertical separations of 6.24 and $3.86 \mu\text{m}$, respectively. The rectangular interstitial regions between the waveguides are denoted by $\mathcal{M}_{13}, \mathcal{M}_{24}, \mathcal{M}_{23}$, and \mathcal{M}_{14} , with the two subscripts indicating the two neighboring waveguides.

In the simple model introduced in Fig. 3(a), the on-site detuning of the four coupled elements is referred to as $\pm\Delta$ [see also Eq. (16)]. Therefore, here we denote the dielectric constant of a waveguide in the *absence* of detuning

or gain/loss as $\epsilon_c = (n_1^2 + n_2^2)/2$, with $\delta \equiv k_0^2(n_1^2 - \epsilon_c)$ and $-\delta = k_0^2(n_2^2 - \epsilon_c)$ playing the role of the on-site detunings. k_0 is defined as ω_0/c using the circular frequency ω_0 of the propagating modes. Because the difference between n_1 and n_2 we consider here is small, we treat δ , as well as all gain and loss parameters, as small perturbations.

We assume that a waveguide with ϵ_c supports a single TE mode with the propagation constant β_0 at ω_0 , i.e., the field evolves as $\exp(i\beta_0 z - i\omega_0 t)$ along the waveguide direction z . In the coupled system, supermodes of the form $\Psi(\mathbf{r}, t) = \phi(\mathbf{r}) \exp(i\beta_0 z - i\omega_0 t)$ satisfy the scalar Helmholtz equation

$$[\nabla_{\perp}^2 + \epsilon(\mathbf{x})k_0^2]\phi(\mathbf{r}) = (\beta_0^2 + 2i\beta_0\partial_z - \partial_z^2)\phi(\mathbf{r}), \quad (\text{B1})$$

where \mathbf{x} is the transverse coordinate, ∇_{\perp}^2 is the transverse Laplacian operator, and $\epsilon(\mathbf{x})$ is the position-dependent dielectric constant. In the paraxial regime, the second-order derivative on the right-hand side can be neglected, leading to a Schrödinger-like equation

$$i\partial_z\phi(\mathbf{r}) = \frac{1}{2\beta_0}[-\nabla_{\perp}^2 + V(\mathbf{x})]\phi(\mathbf{r}), \quad (\text{B2})$$

where the potential energy takes the form $V(\mathbf{x}) = \beta_0^2 - \epsilon(\mathbf{x})k_0^2$ and z plays the role of time. We denote an eigenvalue of the effective Hamiltonian on the right-hand side of Eq. (B2) by λ , which has the same dimension as β_0 . This is the quantity we have plotted in Figs. 3(c) and 3(d). The corresponding eigenstate takes the form $\phi(\mathbf{r}) = \phi(\mathbf{x}) \exp(i\lambda z)$, and we note that the magnitude of λ is much smaller than β_0 in the paraxial regime.

To show that this coupled waveguide system with $\delta \neq 0$ can realize the tight-binding model given by Eq. (16), we introduce gain and loss in the following fashion. First, an imaginary perturbation is added to the dielectric constant in the interstitial regions, with $-ir$ in \mathcal{M}_{13} , \mathcal{M}_{23} and $+ir$ in \mathcal{M}_{24} , \mathcal{M}_{14} . Next, an imaginary perturbation $i\gamma_j$ is added to each waveguide \mathcal{D}_j , and its magnitude depends on whether a real or complex on-site detuning is desired. Finally, we work with the basis of *individual waveguide modes* ψ_j , defined for each stand-alone waveguide in the absence of detuning or gain/loss.

By expanding ϕ in Eq. (B2) in this basis and performing the usual overlapping integrals, we arrive at a matrix Hamiltonian of the following form,

$$\tilde{H} = \begin{pmatrix} \Delta + i\Gamma_1 & & g_1 & \tilde{g}_2 \\ & \Delta + i\Gamma_2 & g_2 & \tilde{g}_1 \\ g_1 & g_2 & -\Delta + i\Gamma_3 & \\ \tilde{g}_2 & \tilde{g}_1 & & -\Delta + i\Gamma_4 \end{pmatrix}, \quad (\text{B3})$$

where the factor $1/2\beta_0$ on the right-hand side of Eq. (B2) is absorbed by defining $\tilde{\epsilon}_c \equiv \epsilon_c/2\beta_0$ and $\tilde{\epsilon}_{cl} \equiv n_{cl}^2/2\beta_0$ as we will show below. Each term in Eq. (B3) is proportional to integrals of the products of waveguide fields $\psi_i\psi_j$ at all perturbed domains. For instance, $\Delta = J\delta$ in the diagonal terms are defined with $J \equiv \int_{\mathcal{D}_1} \tilde{\epsilon}_c \psi_1^2 d\mathbf{x}$, while Γ_j ($j = 1, 2, 3, 4$) are defined as $J\gamma_1 + \Gamma_-$, $J\gamma_2 - \Gamma_-$, $J\gamma_3 + \Gamma_+$, and $J\gamma_4 - \Gamma_+$ respectively, where $\Gamma_{\pm} = r(\rho_1 \pm \rho_2)$, $\rho_1 \equiv \int_{\mathcal{M}_{13}} \tilde{\epsilon}_c \psi_1^2 d\mathbf{x}$,

and $\rho_2 \equiv \int_{\mathcal{M}_{24}} \tilde{\epsilon}_c \psi_1^2 d\mathbf{x}$. The off-diagonal terms (i.e., the couplings) are given by

$$g_1 = \chi j_1 + i[r\kappa_1 + j_1(\gamma_1 + \gamma_3)], \quad (\text{B4})$$

$$\tilde{g}_1 = \chi j_1 - i[r\kappa_1 - j_1(\gamma_2 + \gamma_4)], \quad (\text{B5})$$

$$g_2 = \chi j_2 + i[r\kappa_2 + j_2(\gamma_2 + \gamma_3)], \quad (\text{B6})$$

$$\tilde{g}_2 = \chi j_2 - i[r\kappa_2 - j_2(\gamma_1 + \gamma_4)], \quad (\text{B7})$$

with $\chi \equiv k_0^2(\tilde{\epsilon}_c - \tilde{\epsilon}_{cl})$, $j_1 = \int_{\mathcal{D}_1} \tilde{\epsilon}_c \psi_1 \psi_3 d\mathbf{x}$, $j_2 = \int_{\mathcal{D}_1} \tilde{\epsilon}_c \psi_1 \psi_4 d\mathbf{x}$, $\kappa_1 = \int_{\mathcal{M}_{13}} \tilde{\epsilon}_c \psi_1 \psi_3 d\mathbf{x}$, and $\kappa_2 = \int_{\mathcal{M}_{14}} \tilde{\epsilon}_c \psi_1 \psi_4 d\mathbf{x}$.

Clearly, the form of the matrix of Eq. (B3) resembles that of the model Eq. (16) we intend to reproduce, and they become exactly the same with the following choice of the gain and loss in each waveguide: $\gamma_1 = -\Gamma_-/J$, $\gamma_3 = -\Gamma_+/J$, $\gamma_2 = -\gamma_1$, and $\gamma_4 = -\gamma_3$. With this choice, the diagonal terms of \tilde{H} become a pair of detunings with equal magnitude but opposite signs (i.e., $\pm\Delta$), while the off-diagonal terms now satisfy $g_1 = \tilde{g}_1^*$, $g_2 = \tilde{g}_2^*$ as in Eq. (16):

$$\tilde{H} = \begin{pmatrix} \Delta & & g_1 & \tilde{g}_2^* \\ & \Delta & g_2 & \tilde{g}_1^* \\ g_1^* & g_2^* & -\Delta & \\ & & & -\Delta \end{pmatrix}. \quad (\text{B8})$$

We note that if just to satisfy these requirements of the couplings, a weaker condition $\gamma_1 + \gamma_2 + \gamma_3 + \gamma_4 = 0$ is needed, i.e., with no excessive gain or loss when all four waveguides are considered.

To verify that the tight-binding model derived above captures the coupled waveguides, finite-difference (FD) simulations are carried out at a fixed wavelength of $1.550 \mu\text{m}$. A $19 \mu\text{m} \times 12 \mu\text{m}$ computational domain is used, which is discretized uniformly with rectangular elements $0.29 \mu\text{m} \times 0.28 \mu\text{m}$ in size. Several stages are performed in the simulations.

The first stage solves the Helmholtz equation for a single waveguide of permittivity $\epsilon_c = 2.1287$, from which we obtain the propagation constant $\beta_0 = 5.88 \mu\text{m}^{-1}$ and the field $\psi(\mathbf{x})$. This field is then shifted to the center of each waveguide in the coupled system, which we take as ψ_j and use to compute all the integrals J , j_1 , ρ_1 , κ_1 , j_2 , ρ_2 , and κ_2 .

Here, we also perform two additional steps to improve the accuracy of these quantities. (1) By removing all gain and loss

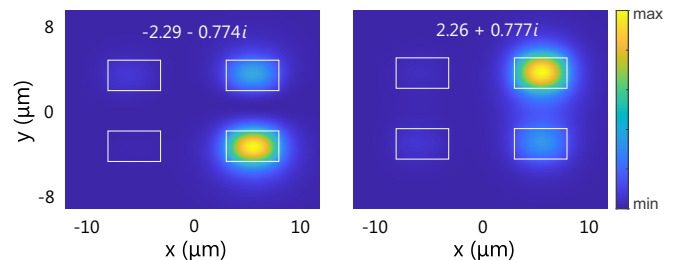


FIG. 6. Intensity patterns of two propagation modes in Fig. 3(d). The insets show their eigenvalues of the paraxial equation in the unit of nm^{-1} .

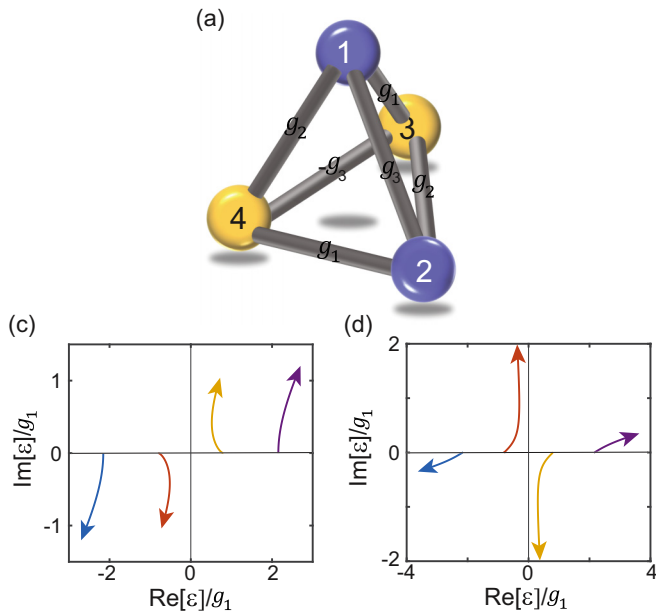


FIG. 7. Non-Hermitian chiral symmetry of a 3D pyramid. (a) Schematic of the system. Purple and orange denote the on-site detunings $\pm\beta$. (b) Its eigenvalue spectrum with $g_2 = g_1 \in \mathbb{R}$, $g_3 = 0.8g_1$, and detuning $\alpha e^{i\pi/4}\gamma^3\gamma^5$, where α is increased from 0 to 2. (c) Same as (d) but with an additional detuning $\alpha e^{i\pi/3}\gamma^1\gamma^2$.

(i.e., setting $\gamma_j = r = 0$), \tilde{H} given by Eq. (B8) still holds but with simplified couplings $g_{1,2} = \tilde{g}_{1,2} = \chi j_{1,2}$. By fitting the result of the FD simulation in this case with \tilde{H} , we find that the fitted values for J and $j_{1,2}$ agree qualitatively with their analytical expressions, with a difference of less than 15% in general. These fitted values are used in later steps. (2) Next, we introduce a fixed $r = r_{\max} = 0.009$, while all the γ 's are still zero in the FD simulation. By fitting the result of the FD simulation in this case with the general \tilde{H} given by Eq. (B3), we find corrections to ρ_1 , ρ_2 , κ_1 , and κ_2 , which are again less than 15% in general.

Finally, the choice of gain and loss that leads to Eq. (B8) is implemented in the FD simulations. Since these values of γ 's in the derived tight-binding model are proportional to r ,

we make a final correction to this constant of proportionality, i.e., multiplying all γ 's by the same factor slightly deviated from 1, in order to produce the best fit of the FD simulation at $r = r_{\max}$. By reducing r (i.e., the amount of gain and loss in the interstitial regions) from r_{\max} and the values of γ 's accordingly, we produce the comparison of the FD simulations and the tight-binding model shown in Figs. 3(c) and 3(d).

In Fig. 6 we also show the intensity patterns of the two eigenmodes in the first and third quadrants of the complex eigenvalue plane at r_{\max} in Fig. 3(d). At first glance, their patterns seem to be mirror images of each other with respect to the horizontal axis. However, their local intensity maxima in each cavity are given by $[0.0583, 1, 0.3332, 0.0327]$ and $[0.0103, 0.3921, 1, 0.0649]$, respectively, which clearly indicates the absence of any mirror symmetry. Here, we have normalized the global intensity maximum to be 1.

APPENDIX C: 3D PYRAMID

To show that the Clifford algebra can still lead to non-Hermitian chiral symmetries without two sublattices and their chiral operator γ^0 , we consider a lattice with such connectivity in Fig. 7(a) and the following Hamiltonian,

$$H = g_1\gamma^5 + g_2\gamma^0\gamma^1 + g_3\gamma^1\gamma^5, \quad (C1)$$

where g_3 represents the two NNN terms. We caution that this model requiring careful matching of the sign and magnitude of three pairs of couplings, and hence it is difficult to realize.

Its chiral symmetries are specified by $\Pi_1 = \gamma^1$ and $\Pi_2 = \gamma^0\gamma^5$, which can be checked using Eqs. (14) and (15). Π_1 tolerates detunings of the forms γ^0 and $\gamma^1\gamma^2$, shown explicitly below Eq. (15). At the same time, Π_2 accommodates detunings given by γ^0 and $\gamma^3\gamma^5$ [Fig. 7(c)]. At first glance, a detuning consisting of a superposition of $\gamma^3\gamma^5$ and $\gamma^1\gamma^2$ (i.e., $H \rightarrow H + d_1\gamma^1\gamma^2 + d_2\gamma^3\gamma^5$) would then lift all chiral symmetries of the system. However, the chiral symmetry given by Π_1 actually evolves with the detuning, i.e.,

$$\Pi_1 \rightarrow \gamma^1 + d_2\gamma^1\gamma^3, \quad (C2)$$

and the non-Hermitian Hamiltonian still has a symmetric spectrum about the origin of the complex energy plane [Fig. 7(d)]. Only by having all three forms of detuning can this chiral symmetry be removed.

-
- [1] R. Shankar, *Principles of Quantum Mechanics*, 2nd ed. (Springer, New York, 1994).
- [2] B. A. Bernevig and T. L. Hughes, *Topological Insulators and Topological Superconductors*, (Princeton University Press, Princeton, NJ, 2013).
- [3] J. D. H. Rivero and L. Ge, Pseudochirality: A Manifestation of Noether's Theorem in Non-Hermitian Systems, *Phys. Rev. Lett.* **125**, 083902 (2020).
- [4] L. Feng, R. El-Ganainy, and L. Ge, Non-Hermitian photonics based on parity-time symmetry, *Nat. Photonics* **11**, 752 (2017).
- [5] R. El-Ganainy, K. G. Makris, M. Khajavikhan, Z. H. Musslimani, S. Rotter, and D. N. Christodoulides, Non-Hermitian physics and PT symmetry, *Nat. Phys.* **14**, 11 (2018).
- [6] V. V. Konotop, J. Yang, and D. A. Zezyulin, Nonlinear waves in \mathcal{PT} -symmetric systems, *Rev. Mod. Phys.* **88**, 035002 (2016).
- [7] C. M. Bender and S. Boettcher, Real Spectra in Non-Hermitian Hamiltonians having \mathcal{PT} Symmetry, *Phys. Rev. Lett.* **80**, 5243 (1998).
- [8] S. Malzard, C. Poli, and H. Schomerus, Topologically Protected Defect States in Open Photonic Systems with Non-Hermitian Charge-Conjugation and Parity-Time Symmetry, *Phys. Rev. Lett.* **115**, 200402 (2015).
- [9] L. Ge, Symmetry-protected zero-mode laser with a tunable spatial profile, *Phys. Rev. A* **95**, 023812 (2017).
- [10] B. Qi, L. Zhang, and L. Ge, Defect States Emerging from a Non-Hermitian Flatband of Photonic Zero Modes, *Phys. Rev. Lett.* **120**, 093901 (2018).

- [11] L. Ge, Non-Hermitian lattices with a flat band and polynomial power increase [Invited], *Photonics Res.* **6**, A10 (2018).
- [12] K. Kawabata, K. Shiozaki, M. Ueda, and M. Sato, Symmetry and Topology in Non-Hermitian Physics, *Phys. Rev. X* **9**, 041015 (2019).
- [13] A. Mostafazadeh, Pseudo-Hermiticity versus PT symmetry: The necessary condition for the reality of the spectrum of a non-Hermitian Hamiltonian, *J. Math. Phys.* **43**, 205 (2002).
- [14] M. Z. Hasan and C. L. Kane, Topological insulators, *Rev. Mod. Phys.* **82**, 3045 (2010).
- [15] X.-L. Qi and S.-C. Zhang, Topological insulators and superconductors, *Rev. Mod. Phys.* **83**, 1057 (2011).
- [16] J. Alicea, New directions in the pursuit of Majorana fermions in solid state systems, *Rep. Prog. Phys.* **75**, 076501 (2012).
- [17] C. W. J. Beenakker, Random-matrix theory of Majorana fermions and topological superconductors, *Rev. Mod. Phys.* **87**, 1037 (2015).
- [18] C. Nayak, S. H. Simon, A. Stern, M. Freedman, and S. Das Sarma, Non-Abelian anyons and topological quantum computation, *Rev. Mod. Phys.* **80**, 1083 (2008).
- [19] S. D. Sarma, M. Freedman, and C. Nayak, Majorana zero modes and topological quantum computation, *npj Quantum Inf.* **1**, 15001 (2015).
- [20] D. Aasen, M. Hell, R. V. Mishmash, A. Higginbotham, J. Danon, M. Leijnse, T. S. Jespersen, J. A. Folk, C. M. Marcus, K. Flensberg, and J. Alicea, Milestones toward Majorana-based quantum computing, *Phys. Rev. X* **6**, 031016 (2016).
- [21] L. Lu, J. D. Joannopoulos, and M. Soljačić, Topological photonics, *Nat. Photonics* **8**, 821 (2014).
- [22] P. St-Jean, V. Goblot, E. Galopin, A. Lemaître, T. Ozawa, L. Le Gratiet, I. Sagnes, J. Bloch, and A. Amo, Lasing in topological edge states of a one-dimensional lattice, *Nat. Photonics* **11**, 651 (2017).
- [23] B. Bahari, A. Ndao, F. Vallini, A. El Amili, Y. Fainman, and B. Kanté, Nonreciprocal lasing in topological cavities of arbitrary geometries, *Science* **358**, 636 (2017).
- [24] M. A. Bandres, S. Wittek, G. Harari, M. Parto, J. Ren, and M. Segev, Topological insulator laser: Experiments, *Science* **359**, eaar4005 (2018).
- [25] H. Zhao, P. Miao, M. H. Teimourpour, S. Malzard, R. El-Ganainy, H. Schomerus, and L. Feng, Topological hybrid silicon microlasers, *Nat. Commun.* **9**, 981 (2018).
- [26] M. Pan, H. Zhao, P. Miao, S. Longhi, and L. Feng, Photonic zero mode in a parity-time symmetric lattice, *Nat. Commun.* **9**, 1308 (2018).
- [27] M. Parto, S. Wittek, H. Hodaei, G. Harari, M. A. Bandres, J. Ren, M. C. Rechtsman, M. Segev, D. N. Christodoulides, and M. Khajavikhan, Complex Edge-State Phase Transitions in 1D Topological Laser Arrays, *Phys. Rev. Lett.* **120**, 113901 (2018).
- [28] D. Leykam, K. Y. Bliokh, C. Huang, Y. D. Chong, and F. Nori, Edge Modes, Degeneracies, and Topological Numbers in Non-Hermitian Systems, *Phys. Rev. Lett.* **118**, 040401 (2017).
- [29] K. Kawabata, S. Higashikawa, Z. Gong, Y. Ashida, and M. Ueda, Topological unification of time-reversal and particle-hole symmetries in non-Hermitian physics, *Nat. Commun.* **10**, 297 (2019).
- [30] T. E. Lee, Anomalous Edge State in a Non-Hermitian Lattice, *Phys. Rev. Lett.* **116**, 133903 (2016).
- [31] C. Yin, H. Jiang, L. Li, R. Lü, and S. Chen, Geometrical meaning of winding number and its characterization of topological phases in one-dimensional chiral non-Hermitian systems, *Phys. Rev. A* **97**, 052115 (2018).
- [32] L. Jin and Z. Song, Bulk-boundary correspondence in a non-Hermitian system in one dimension with chiral inversion symmetry, *Phys. Rev. B* **99**, 081103(R) (2019).
- [33] Y. Xiong, Why does bulk boundary correspondence fail in some non-hermitian topological models, *J. Phys. Commun.* **2**, 035043 (2018).
- [34] S. Yao, F. Song, and Z. Wang, Non-Hermitian Chern Bands, *Phys. Rev. Lett.* **121**, 136802 (2018).
- [35] T. Yoshida, R. Peters, N. Kawakami, and Y. Hatsugai, Symmetry-protected exceptional rings in two-dimensional correlated systems with chiral symmetry, *Phys. Rev. B* **99**, 121101(R) (2019).
- [36] J. Okolowicz, M. Płoszajczak, and I. Rotter, Dynamics of quantum systems embedded in a continuum, *Phys. Rep.* **374**, 271 (2003).
- [37] W. D. Heiss, Exceptional points of non-Hermitian operators, *J. Phys. A: Math. Gen.* **37**, 2455 (2004).
- [38] A. U. Hassan, B. Zhen, M. Soljačić, M. Khajavikhan, and D. N. Christodoulides, Dynamically Encircling Exceptional Points: Exact Evolution and Polarization State Conversion, *Phys. Rev. Lett.* **118**, 093002 (2017).
- [39] C. Dembowski, H.-D. Gräf, H. L. Harney, A. Heine, W. D. Heiss, H. Rehfeld, and A. Richter, Experimental Observation of the Topological Structure of Exceptional Points, *Phys. Rev. Lett.* **86**, 787 (2001).
- [40] S.-B. Lee, J. Yang, S. Moon, S.-Y. Lee, J.-B. Shim, S. W. Kim, J.-H. Lee, and K. An, Observation of an Exceptional Point in a Chaotic Optical Microcavity, *Phys. Rev. Lett.* **103**, 134101 (2009).
- [41] M. Liertzer, L. Ge, A. Cerjan, A. D. Stone, H. E. Türeci, and S. Rotter, Pump-Induced Exceptional Points in Lasers, *Phys. Rev. Lett.* **108**, 173901 (2012).
- [42] R. El-Ganainy, M. Khajavikhan, and L. Ge, Exceptional points and lasing self-termination in photonic molecules, *Phys. Rev. A* **90**, 013802 (2014).
- [43] B. Zhen, C. Wei Hsu, Y. Igarashi, L. Lu, I. Kaminer, A. Pick, S.-L. Chua, J. D. Joannopoulos, and M. Soljačić, Spawning rings of exceptional points out of Dirac cones, *Nature (London)* **525**, 354 (2015).
- [44] G. Scolarici, Pseudo-anti-Hermitian operators in quaternionic quantum mechanics, *J. Phys. A* **35**, 7493 (2002).
- [45] K. Esaki, M. Sato, K. Hasebe, and M. Kohmoto, Edge states and topological phases in non-Hermitian systems, *Phys. Rev. B* **84**, 205128 (2011).
- [46] N. Hatano and D. R. Nelson, Localization Transitions in Non-Hermitian Quantum Mechanics, *Phys. Rev. Lett.* **77**, 570 (1996).
- [47] S. Weidemann, M. Kremer, T. Helbig, T. Hofmann, A. Stegmaier, M. Greiter, R. Thomale, and A. Szameit, Topological funneling of light, *Science* **368**, 311 (2020).
- [48] Z. Zhang, X. Qiao, B. Midya, K. Liu, J. Sun, T. Wu, W. Liu, R. Agarwal, J. M. Jornet, S. Longhi, N. M. Litchinitser, and L. Feng, Tunable topological charge vortex microlaser, *Science* **368**, 760 (2020).
- [49] S. Weinberg, *The Quantum Theory of Fields, Vol. 1: Foundations* (Cambridge University, New York, 2005).
- [50] W. P. Su, J. R. Schrieffer, and A. J. Heeger, Solitons in Polyacetylene, *Phys. Rev. Lett.* **42**, 1698 (1979).

- [51] L. Ge and A. D. Stone, Parity-Time Symmetry Breaking beyond One Dimension: The Role of Degeneracy, *Phys. Rev. X* **4**, 031011 (2014).
- [52] L. Ge, K. G. Makris, D. N. Christodoulides, and L. Feng, Scattering in \mathcal{PT} - and \mathcal{RT} -symmetric multimode waveguides: Generalized conservation laws and spontaneous symmetry breaking beyond one dimension, *Phys. Rev. A* **92**, 062135 (2015).
- [53] L. Ge, Constructing the scattering matrix for optical microcavities as a nonlocal boundary value problem, *Photonics Res.* **5**, B20 (2017).
- [54] S. Longhi, D. Gatti, and G. Della Valle, Robust light transport in non-Hermitian photonic lattices, *Sci. Rep.* **5**, 13376 (2015).
- [55] G. Demange and E.-M. Graefe, Signatures of three coalescing eigenfunctions, *J. Phys. A: Math. Theor.* **45**, 025303 (2012).
- [56] L. Ge, Parity-time symmetry in a flat-band system, *Phys. Rev. A* **92**, 052103 (2015).
- [57] Z. Lin, A. Pick, M. Lončar, and A. W. Rodriguez, Enhanced Spontaneous Emission at Third-Order Dirac Exceptional Points in Inverse-Designed Photonic Crystals, *Phys. Rev. Lett.* **117**, 107402 (2016).
- [58] H. Hodaei, A. U. Hassan, S. Wittek, H. Garcia-Gracia, R. El-Ganainy, D. N. Christodoulides, and M. Khajavikhan, Enhanced sensitivity at higher-order exceptional points, *Nature (London)* **548**, 187 (2017).
- [59] J. Wiersig, Enhancing the Sensitivity of Frequency and Energy Splitting Detection by Using Exceptional Points: Application to Microcavity Sensors for Single-Particle Detection, *Phys. Rev. Lett.* **112**, 203901 (2014).
- [60] W. Chen, Ş. K. Özdemir, G. Zhao, J. Wiersig, and L. Yang, Exceptional points enhance sensing in an optical microcavity, *Nature (London)* **548**, 192 (2017).
- [61] X. Zhou, S. K. Gupta, Z. Huang, Z. Yan, P. Zhan, Z. Chen, M. Lu, and Z. Wang, Optical lattices with higher-order exceptional points by non-Hermitian coupling, *Appl. Phys. Lett.* **113**, 101108 (2018).
- [62] M. J. Rice and E. J. Mele, Elementary Excitations of a Linearly Conjugated Diatomic Polymer, *Phys. Rev. Lett.* **49**, 1455 (1982).
- [63] N. V. Alexeeva, I. V. Barashenkov, K. Rayanov, and S. Flach, Actively coupled optical waveguides, *Phys. Rev. A* **89**, 013848 (2014).
- [64] J. Arkininstall, M. H. Teimourpour, L. Feng, R. El-Ganainy, and H. Schomerus, Topological tight-binding models from nontrivial square roots, *Phys. Rev. B* **95**, 165109 (2017).
- [65] Z. Zhang, M. H. Teimourpour, J. Arkininstall, M. Pan, P. Miao, H. Schomerus, R. El-Ganainy, and L. Feng, Experimental realization of multiple topological edge states in a 1D photonic lattice, *Laser Photonics Rev.* **13**, 1800202 (2019).
- [66] R. Keil, C. Poli, M. Heinrich, J. Arkininstall, G. Weihs, H. Schomerus, and A. Szameit, Universal Sign Control of Coupling in Tight-Binding Lattices, *Phys. Rev. Lett.* **116**, 213901 (2016).
- [67] B. Redding, L. Ge, Q. Song, J. Wiersig, G. S. Solomon, and H. Cao, Local Chirality of Optical Resonances in Ultrasmall Resonators, *Phys. Rev. Lett.* **108**, 253902 (2012).
- [68] R. Sarma, L. Ge, J. Wiersig, and H. Cao, Rotating Optical Microcavities with Broken Chiral Symmetry, *Phys. Rev. Lett.* **114**, 053903 (2015).
- [69] Q.-T. Cao, H. Wang, C.-H. Dong, H. Jing, R.-S. Liu, X. Chen, L. Ge, Q. Gong, and Y.-F. Xiao, Experimental Demonstration of Spontaneous Chirality in a Nonlinear Microresonator, *Phys. Rev. Lett.* **118**, 033901 (2017).
- [70] S. Liu, J. Wiersig, W. Sun, Y. Fan, L. Ge, J. Yang, S. Xiao, Q. Song, and H. Cao, Transporting the optical chirality through the dynamical barriers in optical microcavities, *Laser Photonics Rev.* **12**, 1800027 (2018).